

DOF and Kinematic Analysis of a Deployable Truss Antenna Assembled by Tetrahedral Elements

Wenlan Liu, Yundou Xu, Yongsheng Zhao, Jiantao Yao, Bo Han and Liangliang Chen

Abstract Deployable structure has played a more and more important role in the large-caliber antennas. This paper deals with the degree of freedom (DOF) and kinematics of a kind of deployable truss antenna composed of tetrahedral elements. Firstly, based on the reciprocal screw theory the DOF of one tetrahedral element is analyzed. Then, the equivalent mechanism of the minimum composite unit of the deployable truss antenna is obtained according to the characteristic of the DOF of the tetrahedral element. Sequentially, the DOF of the deployable truss antenna is derived. Further, the analytical expressions of the positions and velocities of the connection nodes of the antenna during its deploying/folding process are formulated by resorting to the coordinate transformation matrices. Finally, the correctness of the kinematic analysis of the deployable truss antenna is verified by simulation based on the Adams software.

Keywords Deployable structure · Truss antenna · Degree of freedom · Kinematic analysis · Screw theory

W. Liu · Y. Xu (✉) · Y. Zhao · J. Yao · B. Han · L. Chen
Parallel Robot and Mechatronic System Laboratory of Hebei Province,
Qinhuangdao 066004, Hebei, China
e-mail: ydxu@ysu.edu.cn

W. Liu
e-mail: wenlanl@163.com

Y. Zhao
e-mail: yszhao@ysu.edu.cn

J. Yao
e-mail: jtyao@ysu.edu.cn

B. Han
e-mail: 1440731168@qq.com

L. Chen
e-mail: 1307152110@qq.com

Y. Xu · Y. Zhao · J. Yao
Key Laboratory of Advanced Forging and Stamping Technology and Science
of Ministry of National Education Yanshan University, Qinhuangdao 066004, Hebei, China

1 Introduction

Demand for the large-caliber antennas is increasing with the rapid development of the aerospace science and technology. However, the caliber of antennas is severely restricted by limited volume of the launch vehicle. As a result, spatial deployable structures have been widely applied in the large-caliber antennas [1, 2], which have the advantages including higher precision, smaller launch volume and higher reliability for deployment. Basically, deployable antennas can be divided into three categories: mesh, solid surface and inflatable antennas, among which the mesh antenna is the most common type.

The mesh antenna is mainly composed of a reflective metallic mesh and a deployable supporting structure. For this kind of antennas, the most critical part is the deployable supporting structure. There is a large amount of literatures focusing on the deployable structures at present. Wang et al. [3] proposed a two-step topology structure synthesis approach to design novel pyramid deployable truss structures. A structure-electronic synthesis design method of antennas is given in [4]. The literatures [5–8] paid attention to the configuration design of polyhedral linkage for deployable truss structure. Zheng et al. [9] proposed a new conceptual structure design for large deployable spaceborne antennas based on a folded fixed truss hoop reflector. You [10] demonstrated a generic solution for construction of deployable structures in any shape of rotational symmetry. The optimization of antennas was demonstrated in [11, 12]. Besides, Yu et al. [13] accomplished the motion analysis of deployable structures using the finite particle method. Moore-Penrose generalized inverse method is applied to the kinematic analysis of deployable toroidal spatial truss structures for large mesh antenna [14]. Xu et al. [15, 16] addressed the structural design, kinematic and static analysis of a double-ring deployable antenna. What's more, Li et al. [17] used the absolute nodal coordinate formulation to analyze the flexible body dynamics of deployable structures under different temperatures to simulate space environments. Afterwards, Li [18] presented the kinematic, dynamic analysis and control methods of a hoop deployable antenna.

To sum up, most of the above-mentioned literatures focused on the structural design, kinematic and dynamic analysis of deployable structures. There are few investigations on the methods for degree of freedom (DOF) analysis of the deployable structures applied in the antennas. It is well known that getting the number of the DOFs for mechanisms is the most fundamental understanding to a mechanism. However, deployable antenna structure is constituted by a large number of deployable elements through some regular structural topology, which increases the complexity and difficulty of the mobility analysis for this kind of deployable structures. In this work, the DOF of a deployable structure assembled by tetrahedral elements for space truss antennas is analyzed based on the reciprocal screw theory, and the correctness of the mobility analysis is verified by simulation.

2 DOF Analysis of the Deployable Truss Antenna

2.1 Structure of the Deployable Truss Antenna

The deployable truss antenna consists of a large number of basic tetrahedral elements, as shown in Fig. 1. Each tetrahedral element contains four connection nodes, three swing-struts with identical length, and three foldable and deployable struts. Both ends of the struts are connected to the nodes by revolute joints (R), and each foldable and deployable strut is made up of two struts with identical length connected by an R joint, as shown in Fig. 2. For the purpose of analysis, the tetrahedral element shown in Fig. 2 is denoted by $H-ABC$, where the letter H represents the top node and the other letters denote the three nodes located at the undersurface of the tetrahedral element. The axes of all R joints of the tetrahedral element $H-ABC$ are respectively denoted by S_i ($i = 1, 2, \dots, 15$). Then, the geometric characteristics of the S_i can be expressed as: $S_1 \parallel S_2 \parallel S_3 \perp AB$, $S_4 \parallel S_5 \parallel S_6 \perp AC$, $S_7 \parallel S_8 \parallel S_9 \perp BC$, $S_{10} \parallel S_{11} \perp AH$, $S_{12} \parallel S_{13} \perp CH$, and $S_{14} \parallel S_{15} \perp BH$. Besides, the S_{11} , S_{13} and S_{15}

Fig. 1 Deployable truss antenna

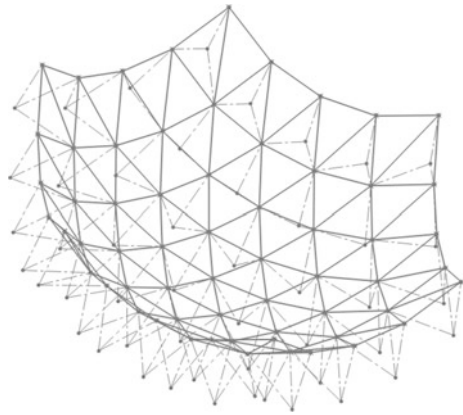


Fig. 2 Schematic diagram of the tetrahedral element

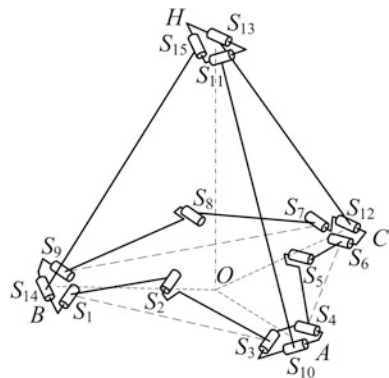


Fig. 3 Schematic diagram of the minimum composite unit

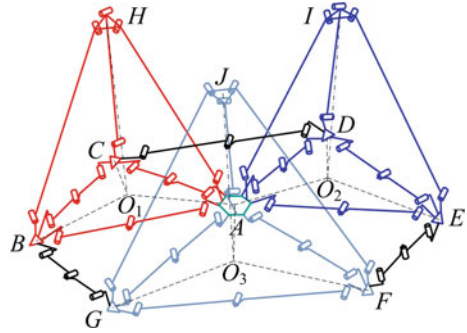
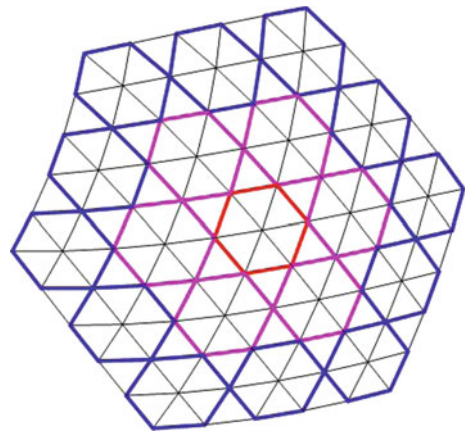


Fig. 4 Reflecting surface of the antenna spliced by the minimum composite units



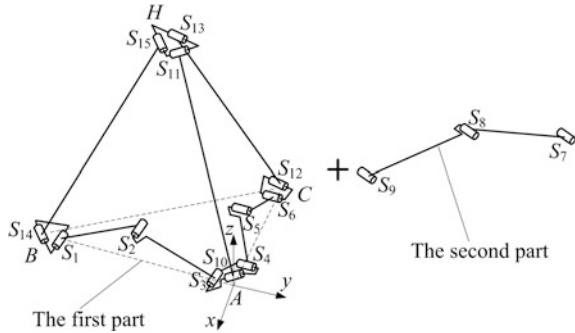
are coplanar and perpendicular to the planes AOH , COH and BOH , respectively, where the point O represents the circumcenter of the triangle ABC .

The minimum composite unit of the deployable truss antenna is constituted by three tetrahedral elements, as shown in Fig. 3. Then the whole deployable truss antenna shown in Fig. 1 can be obtained by extending the minimum composite units from the central axis of the antenna. The reflecting surface of the antenna spliced by the minimum composite units is shown in Fig. 4, in which the triangle planes are the undersurface of the tetrahedral elements and the color hexagons represent the minimum composite units.

2.2 DOF Analysis of the Tetrahedral Element

In order to analyze the DOF of the tetrahedral element, it is firstly divided into two parts in this section, as shown in Fig. 5. Then, the DOF of the first part is derived

Fig. 5 Two parts of the tetrahedral element



based on the reciprocal screw theory. Finally, the DOF of the tetrahedral element can be obtained after considering the constraint influence of the second part.

The first part of the tetrahedral element can be regarded as a parallel mechanism (PM) composed of a fixed node A, a moving node B, and two supporting limbs. One limb connects the node B to the node A by three R joints (i.e., S₁, S₂ and S₃), denoted by the limb RRR. The other limb consists of a closed-loop kinematic chain containing seven R joints (i.e., S₄, S₅, S₆, S₁₂, S₁₃, S₁₁ and S₁₀) and a serial chain RR (i.e., S₁₄ and S₁₅), denoted by the limb (7R)-RR. A fixed coordinate frame A-xyz is attached to the center of the node A, with x-axis perpendicular to the BA, y-axis pointing along the BA, and z-axis determined by the right-hand rule, as shown in Fig. 5.

The closed-loop kinematic chain in the limb (7R)-RR can also be treated as a PM containing a fixed node A, a moving node H, two supporting limbs, RR (i.e., S₁₀ and S₁₁) and RRRRR (i.e., S₄, S₅, S₆, S₁₂ and S₁₃). The constraint wrenches imposed on the node H by the limbs RR and RRRRR can be expressed in the A-xyz as

$$\begin{cases} \mathcal{S}_{r1}^H = (0 \ 0 \ 0 \ 0 \ 0 \ 1)^T \\ \mathcal{S}_{r2}^H = (0 \ 0 \ 0 \ -b_4 \ a_4 \ 0)^T \\ \mathcal{S}_{r3}^H = (x_{11} - x_{10} \ y_{11} - y_{10} \ z_{11} - z_{10} \ y_{10}z_{11} - y_{11}z_{10} \ x_{11}z_{10} - x_{10}z_{11} \ x_{10}y_{11} - x_{11}y_{10})^T, \\ \mathcal{S}_{r4}^H = (a_4 \ b_4 \ 0 \ -b_4z_{10} \ a_4z_{10} \ x_{10}b_4 - a_4y_{10})^T \\ \mathcal{S}_{r5}^H = (0 \ 0 \ 0 \ b_5c_2 \ -a_5c_2 \ a_5b_2 - a_2b_5)^T \end{cases} \tag{1}$$

where, (a₂ b₂ c₂), (a₄ b₄ 0) and (a₅ b₅ 0) denote the direction vectors of the S₄, S₁₀ and S₁₂, (x₁₀ y₁₀ z₁₀) and (x₁₁ y₁₁ z₁₁) represent the position vectors of the centers of the joints S₁₀ and S₁₁, respectively.

The twist of the node H which is reciprocal to the constraint wrenches shown in Eq. (1) is solved as

$$\mathcal{S}_m^H = (0 \ 0 \ 0 \ b_4(z_{11} - z_{10}) \ -a_4(z_{11} - z_{10}) \ b_4(x_{10} - x_{11}) + a_4(y_{11} - y_{10}))^T, \quad (2)$$

where, \mathcal{S}_m^H represents a translation perpendicular to both the \mathcal{S}_{10} and the $\mathcal{A}H$.

It can be known from Eq. (2) that the closed-loop kinematic chain within the limb (7R)-RR is equivalent to a translation joint P, so that the limb (7R)-RR can be substituted by the limb PRR. The constraint wrenches imposed on the node B by the limb PRR can be obtained as

$$\begin{cases} \mathcal{S}_{r1}^1 = (0 \ 0 \ 0 \ 0 \ 0 \ 1)^T \\ \mathcal{S}_{r2}^1 = (0 \ 0 \ 0 \ b_4 \ a_4 \ 0)^T \\ \mathcal{S}_{r3}^1 = (a \ 0 \ c \ (y_{10} + y_{14})c/2 \ az_{10} - ((y_{14} - y_{10})a_4 / (2b_4) + x_{10})c \ -(y_{10} + y_{14})a/2)^T \end{cases}, \quad (3)$$

where, $a = b_4(x_{11} - x_{10}) - a_4(y_{11} - y_{10})$, $c = b_4(z_{11} - z_{10})$, and $y_{10} + y_{14} = y_{11} + y_{15}$, \mathcal{S}_{r1}^1 represents the constraint couple parallel to the z -axis, \mathcal{S}_{r2}^1 is the constraint couple located in the plane xAy and perpendicular to the \mathcal{S}_{14} , and \mathcal{S}_{r3}^1 denotes the constraint force passing through the point $(\frac{(y_{14} - y_{10})a_4}{2b_4} + x_{10} \ \frac{y_{10} + y_{14}}{2}z_{10})$ and along the direction $(a \ 0 \ c)$, in which $(x_{10} \ y_{14} \ z_{10})$ and $(x_{11} \ y_{15} \ z_{11})$ represent the position vectors of the centers of the joints S_{14} and S_{15} , respectively.

Similarly, the constraint wrenches imposed on the node B by the limb RRR can be derived as

$$\begin{cases} \mathcal{S}_{r1}^2 = (0 \ 0 \ 0 \ 0 \ 1 \ 0)^T \\ \mathcal{S}_{r2}^2 = (0 \ 0 \ 0 \ -c_1 \ 0 \ a_1)^T \\ \mathcal{S}_{r3}^2 = (a_1 \ 0 \ c_1 \ y_1c_1 \ 0 \ -a_1y_1)^T \end{cases}, \quad (4)$$

where, $(a_1 \ 0 \ c_1)$ denotes the direction vector of the \mathcal{S}_1 , $(x_1 \ y_1 \ 0)$ represents the position vector of the center of the joint S_1 , \mathcal{S}_{r1}^2 represents the constraint couple parallel to the y -axis, \mathcal{S}_{r2}^2 is the constraint couple located in the plane xAz and perpendicular to the \mathcal{S}_1 , and \mathcal{S}_{r3}^2 is the constraint force passing through the point $(0 \ y_1 \ 0)$ and parallel to the \mathcal{S}_1 .

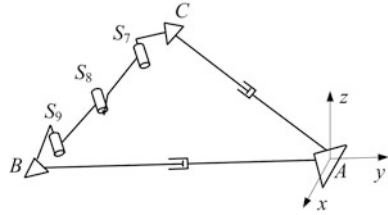
By combining Eqs. (3) and (4) all constraint wrenches suffered by the node B can be obtained. According to the reciprocal screw theory the twist of the node B can be derived as

$$\mathcal{S}_m^B = (0 \ 0 \ 0 \ 0 \ 1 \ 0)^T, \quad (5)$$

where \mathcal{S}_m^B represents a translation along the y -axis, which shows that the node B has a translational DOF with respect to the fixed node A .

As similar as the above solving process, it can be known that the node C also has a translational DOF with respect to the node A . On the condition of considering the

Fig. 6 Equivalent mechanism of the tetrahedral element



constraint influence of the second part of the tetrahedral element, the tetrahedral element can be equivalent to the mechanism shown in Fig. 6. It can be easily obtained that the number of the DOFs of the equivalent mechanism is one.

2.3 DOF of the Deployable Truss Antenna

According to the analysis in Sect. 2.2 the equivalent mechanism of the minimum composite unit shown in Fig. 2 can also be formulated, as shown in Fig. 7.

Assuming that the foldable and deployable strut BG is removed from the equivalent mechanism shown in Fig. 7 and the joint connecting the node B to the node A is selected as the actuated joint, then the nodes C, D, E, F and G will move as the movement of the node B , as shown in Fig. 8. According to the characteristic of the DOF of the tetrahedral element there exist the following relations:

$$\frac{AB_1}{AB} = \frac{AC_1}{AC} = \frac{AD_1}{AD} = \frac{AE_1}{AE} = \frac{AF_1}{AF} = \frac{AG_1}{AG}. \tag{6}$$

Fig. 7 Equivalent mechanism of the minimum composite unit

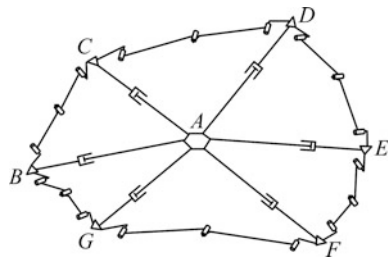
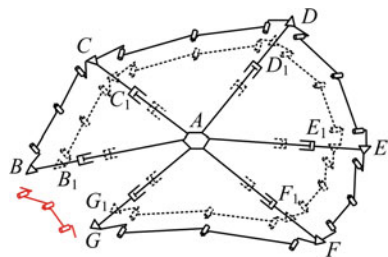


Fig. 8 Configuration of the mechanism shown in this figure after movement



From Eq. (6) it can be gotten that $\frac{AB_1}{AB} = \frac{AG_1}{AG}$, which will not be restricted after connecting the foldable and deployable strut BG to the nodes B and G . Therefore, the minimum composite unit also has one DOF.

Based on the structural topology relationship of the minimum composite unit, we can derive that the number of the DOFs of the whole deployable truss antenna shown in Fig. 1 also is one. That is to say, only the positions of the connection nodes of the deployable truss antenna are changing during its deploying/folding process, but their orientations keep constant.

3 Kinematic Analysis of the Deployable Truss Antenna

3.1 Position and Velocity Analysis of the Tetrahedral Element

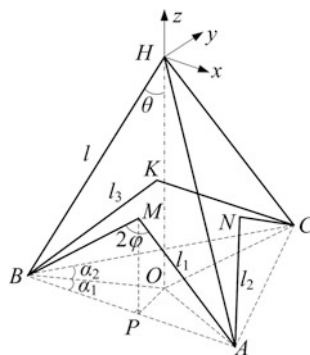
It can be known from the analysis mentioned in Sect. 2 that the orientations of the connection nodes are unchangeable during the deploying/folding process of the antenna. Consequently, the kinematic sketch shown in Fig. 9 is used to analyze the position and velocity variations of the nodes of the tetrahedral element.

As shown in Fig. 9, a reference coordinate system $H-xyz$ is attached to the node H with x -axis parallel to the BA and z -axis along the OH . Then the following equation can be obtained:

$$BP = l_1 \sin \varphi, BO = AO = CO = \frac{l_1}{\cos \alpha_1} \sin \varphi, PO = l_1 \tan \alpha_1 \sin \varphi, \quad (7)$$

where, $\cos \alpha_1 = l_1 \sin(\alpha_1 + \alpha_2)/l_2$, $\cos(\alpha_1 + \alpha_2) = (l_1^2 + l_3^2 - l_2^2)/(2l_1l_3)$, l_1 , l_2 and l_3 represent the length of the struts AM (BM), AN (CN) and BK (CK), respectively, φ denotes half of the angle between the BM and AM , α_1 (α_2) is the constant angle between the BO and BA (BC).

Fig. 9 Kinematic sketch of the tetrahedral element



Besides, there exists that

$$\sin \theta = \frac{BO}{BH} = \frac{l_1}{l \cos \alpha_1} \sin \varphi, \quad OH = l \cos \theta, \quad (8)$$

in which l denotes the length of the swing-struts HA , HB and HC .

Then the position vectors of the nodes A , B and C expressed in the H -xyz can be derived as

$$\begin{cases} \mathbf{P}_A = (l_1 \sin \varphi - l_1 \tan \alpha_1 \sin \varphi - l \cos \theta)^T \\ \mathbf{P}_B = (-l_1 \sin \varphi \quad -l_1 \tan \alpha_1 \sin \varphi \quad -l \cos \theta)^T \\ \mathbf{P}_C = (l_1 \cos \beta \sin \varphi / \cos \alpha_1 \quad l_1 \sin \beta \sin \varphi / \cos \alpha_1 \quad -l \cos \theta)^T \end{cases}, \quad (9)$$

where $\beta = 2\alpha_2 + \alpha_1$.

The angular velocities of the swing-struts HA , HB and HC can be computed by

$$\begin{cases} \boldsymbol{\omega}_{HA} = \mathbf{r}_1 \dot{\theta} = (\sin \alpha_1 \quad \cos \alpha_1 \quad 0)^T \dot{\theta} \\ \boldsymbol{\omega}_{HB} = \mathbf{r}_2 \dot{\theta} = (\sin \alpha_1 \quad -\cos \alpha_1 \quad 0)^T \dot{\theta}, \\ \boldsymbol{\omega}_{HC} = \mathbf{r}_3 \dot{\theta} = (-\sin \beta \quad \cos \beta \quad 0)^T \dot{\theta} \end{cases} \quad (10)$$

where, \mathbf{r}_1 , \mathbf{r}_2 and \mathbf{r}_3 represent the unit normal vectors of the planes AOH , BOH and COH , respectively, and $\dot{\theta}$ can be gotten by taking the derivative of Eq. (8) with respect to time as

$$\dot{\theta} = \frac{l_1 \cos \varphi}{l \cos \alpha_1 \cos \theta} \dot{\varphi}. \quad (11)$$

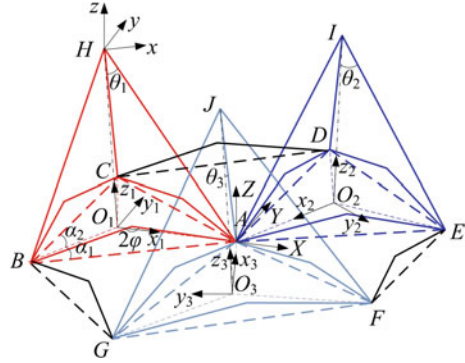
On the basis of Eqs. (9) and (10) the velocities of the nodes A , B and C can be calculated as

$$\begin{cases} \mathbf{V}_A = \boldsymbol{\omega}_{HA} \times \mathbf{P}_A = (-l \cos \theta \cos \alpha_1 \quad l \cos \theta \sin \alpha_1 \quad -l_1 \sin \varphi (\tan \alpha_1 \sin \alpha_1 + \cos \alpha_1))^T \cdot \frac{l_1 \cos \varphi}{l \cos \alpha_1 \cos \theta} \dot{\varphi} \\ \mathbf{V}_B = \boldsymbol{\omega}_{HB} \times \mathbf{P}_B = (l \cos \theta \cos \alpha_1 \quad l \cos \theta \sin \alpha_1 \quad -l_1 \sin \varphi (\tan \alpha_1 \sin \alpha_1 + \cos \alpha_1))^T \cdot \frac{l_1 \cos \varphi}{l \cos \alpha_1 \cos \theta} \dot{\varphi} \\ \mathbf{V}_C = \boldsymbol{\omega}_{HC} \times \mathbf{P}_C = -(l \cos \theta \cos \beta \quad l \cos \theta \sin \beta \quad \frac{l_1 \sin \varphi}{\cos \alpha_1})^T \cdot \frac{l_1 \cos \varphi}{l \cos \alpha_1 \cos \theta} \dot{\varphi} \end{cases}. \quad (12)$$

3.2 Position and Velocity Analysis of the Minimum Composite Unit

The kinematic sketch of the minimum composite unit is shown in Fig. 10. A reference coordinate system A -XYZ is attached to the node A with Z -axis being

Fig. 10 Kinematic sketch of the minimum composite unit



vertically placed and X -axis located in the plane AO_1H and having an angle γ_1 with respect to the AO_1 . Three body-fixed coordinate frames $O_j-x_jy_jz_j$ ($j = 1,2,3$) are assigned at the circumcenters O_j of the triangles ABC , ADE and AFG , with x_j -axis coinciding with the O_1A , O_2A and O_3A , and z_j -axis point along the O_1H , O_2I and O_3J , respectively, and y_j -axis are determined by the right-hand rule.

In the light of the analysis in Sect. 3.1 the position vectors of the nodes B , C and H expressed in the $O_1-x_1y_1z_1$ are

$$\begin{cases} {}^{O_1}P_H = (0 \quad 0 \quad l \cos \theta_1)^T \\ {}^{O_1}P_B = {}^{O_1}R \cdot {}^H P_B + {}^{O_1}P_H = l_1 \sin \varphi (M_1 \quad -2 \sin \alpha_1 \quad 0)^T \\ {}^{O_1}P_C = {}^{O_1}R \cdot {}^H P_C + {}^{O_1}P_H = l_1 \sin \varphi (M_2 \quad \cos \beta \tan \alpha_1 + \sin \beta \quad 0)^T \end{cases}, \quad (13)$$

in which, $M_1 = \tan \alpha_1 \sin \alpha_1 - \cos \alpha_1$ and $M_2 = \cos \beta - \sin \beta \tan \alpha_1$, ${}^H P_B$ and ${}^H P_C$ represent the position vectors of the nodes B and C expressed in the H - xyz , respectively, ${}^{O_1}R$ is the orientation matrix of the H - xyz with respect to the $O_1-x_1y_1z_1$, which can be formulated by ${}^{O_1}R = R(z, \alpha_1)$.

By resorting to the coordinate transformation matrix the position vectors of the nodes B , C and H can be expressed in the A - XYZ as

$$\begin{cases} {}^A P_H = {}^A_{O_1}R \cdot {}^{O_1}P_H + {}^A P_{O_1} \\ {}^A P_B = {}^A_{O_1}R \cdot {}^{O_1}P_B + {}^A P_{O_1}, \\ {}^A P_C = {}^A_{O_1}R \cdot {}^{O_1}P_C + {}^A P_{O_1} \end{cases}, \quad (14)$$

where, ${}^A_{O_1}R$ is the orientation matrix of the $O_1-x_1y_1z_1$ with respect to the A - XYZ , which can be computed by ${}^A_{O_1}R = R(Y, \gamma_1)$, and ${}^A P_{O_1}$ is the position vector of the point O_1 expressed in the A - XYZ , which can be calculated by

$${}^A\mathbf{P}_{O_1} = -{}^A_{O_1}\mathbf{R}{}^{O_1}\mathbf{P}_A = -{}^A_{O_1}\mathbf{R}(\mathbf{A}O_1 \quad 0 \quad 0) = \left(-\frac{l_1 \cos \gamma_1}{\cos \alpha_1} \sin \varphi \quad 0 \quad \frac{l_1 \sin \gamma_1}{\cos \alpha_1} \sin \varphi \right). \quad (15)$$

Substituting Eqs. (13) and (15) into Eq. (14) yields

$$\begin{cases} {}^A\mathbf{P}_H = \left(l \sin \gamma_1 \cos \theta_1 - \frac{l_1 \cos \gamma_1}{\cos \alpha_1} \sin \varphi \quad 0 \quad l \cos \gamma_1 \cos \theta_1 + \frac{l_1 \sin \gamma_1}{\cos \alpha_1} \sin \varphi \right)^T \\ {}^A\mathbf{P}_B = l_1 \sin \varphi \left(M_1 \cos \gamma_1 - \frac{\cos \gamma_1}{\cos \alpha_1} \quad -2 \sin \alpha_1 \quad \frac{\sin \gamma_1}{\cos \alpha_1} - M_1 \sin \gamma_1 \right)^T \\ {}^A\mathbf{P}_C = l_1 \sin \varphi \left(M_2 \cos \gamma_1 - \frac{\cos \gamma_1}{\cos \alpha_1} \quad \cos \beta \tan \alpha_1 + \sin \beta \quad \frac{\sin \gamma_1}{\cos \alpha_1} - M_2 \sin \gamma_1 \right)^T \end{cases}. \quad (16)$$

Then taking the derivative of Eq. (16) with respect to time and taking Eq. (11) in mind leads to

$$\begin{cases} {}^A\mathbf{V}_H = \left(-\sin \gamma_1 \tan \theta_1 - \cos \gamma_1 \quad 0 \quad \sin \gamma_1 - \cos \gamma_1 \tan \theta_1 \right)^T \frac{l_1}{\cos \alpha_1} \cos \varphi \dot{\varphi} \\ {}^A\mathbf{V}_B = \left(M_1 \cos \gamma_1 - \frac{\cos \gamma_1}{\cos \alpha_1} \quad -2 \sin \alpha_1 \quad \frac{\sin \gamma_1}{\cos \alpha_1} - M_1 \sin \gamma_1 \right)^T l_1 \cos \varphi \dot{\varphi} \\ {}^A\mathbf{V}_C = \left(M_2 \cos \gamma_1 - \frac{\cos \gamma_1}{\cos \alpha_1} \quad \cos \beta \tan \alpha_1 + \sin \beta \quad \frac{\sin \gamma_1}{\cos \alpha_1} - M_2 \sin \gamma_1 \right)^T l_1 \cos \varphi \dot{\varphi} \end{cases}, \quad (17)$$

which just are the velocity vectors of the nodes H , B and C during the deploying/folding process of the minimum composite unit.

In the same way, the position and velocity vectors of the remaining nodes of the minimum composite unit can be derived. Thus, in view of the structural topology relationship of the minimum composite units and the coordinate transform matrices, the kinematic analysis of the whole antenna can be easily accomplished.

4 Numerical Calculation and Simulation Verification

4.1 Verification on the DOF Analysis

The simulation model of a deployable truss spherical antenna composed of 27 tetrahedral elements is shown in Fig. 11. On the condition that one of the R joints of the 27 tetrahedral elements is actuated, the deployable truss antenna can be completely folded, as shown in Fig. 12, which effectively verifies the correctness of the DOF analysis of the deployable truss antenna.

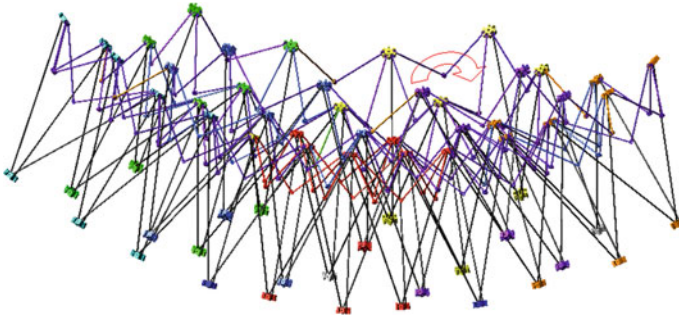


Fig. 11 Deployable truss antenna composed of 27 tetrahedral elements

Fig. 12 Folded configuration of the antenna



4.2 Verification on the Kinematic Analysis

A set of structure parameters of the minimum composite unit are given as: $l = 0.59$ m, $l_1 = l_2 = 0.250376$ m, $l_3 = 0.25$ m, and $\gamma_1 = \gamma_2 = \gamma_3 = 3.623^\circ$, where γ_2 (γ_3) represents the angle between the O_2A (O_3A) and the plane XAY . The minimum composite unit is folded from the initial configuration with $\varphi_0 = 66.829^\circ$. Let $\varphi = \varphi_0 - 0.5^\circ t$, then the simulation values of the positions and velocities of all nodes can be measured by the Adams software. The theoretical value and simulation result of the position variation of the node F and that of the velocity variation of the node I are given in Fig. 13 as representatives.

It can be seen from Fig. 13 that the simulation results and the theoretical values of the nodes F and I are basically consistent, and the errors between the theoretical values and the simulation ones of all nodes are less than 2 %, which effectively shows the correctness of the kinematic analysis of the deployable truss antenna.

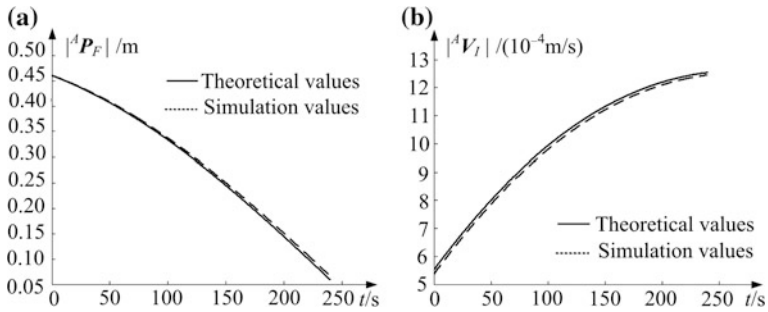


Fig. 13 **a** Position variation of the node F , **b** Velocity variation of the node I

5 Conclusions

In this work, an approach based on the reciprocal screw theory for the DOF analysis of the deployable truss antenna assembled by tetrahedral elements is presented, which greatly reduces the complexity and difficulty on the mobility analysis of this kind of mechanisms with multiple coupling-loops. The tetrahedral element is divided into a PM and a serial kinematic chain. On the basis of the numbers and characteristic of the DOF of the divided PM, the tetrahedral element with multiple coupling-loops is converted to a single-loop mechanism, as a result, the minimum composite unit of the antenna is also simplified, which contributes to the investigation on the DOF of the whole deployable truss antenna. In addition, according to the topological relationship of the antenna and the coordinate transformation matrices the position and velocity vectors of the connection nodes of the antenna during its deploying/folding process are derived. What's more, the simulation model of a deployable truss spherical antenna composed of 27 tetrahedral elements is built, and the simulation results on the DOF and kinematics of the antenna indicate the correctness of the theoretical analysis.

In view of the folded configuration of the deployable truss antenna shown in Fig. 13, future works are suggested: if the tetrahedral element mentioned in this paper is applied to the curved antenna, such as, parabolic or spherical antenna, a portion of R joints of the tetrahedral element need to be changed in order to achieve a smaller stowed volume.

Acknowledgments This research was sponsored by the National Natural Science Foundation of China under Grant 51675458 and Grant 51275439.

References

1. Cherniavsky AG, Gulyayev VI, Gaidaichuk VV, Fedoseev AI (2005) Large deployable space antennas based on usage of polygonal pantograph. *J Aerosp Eng* 18:139–145
2. Fazli N, Abedian A (2011) Design of tensegrity structures for supporting deployable mesh antennas. *Sci Iran* 18:1078–1087
3. Wang Y, Deng ZQ, Liu RQ, Yang H, Guo HW (2014) Topology structure synthesis and analysis of spatial pyramid deployable truss structures for satellite SAR antenna. *Chin J Mech Eng Engl Ed* 27:683–692
4. Xu Y, Guan FL (2013) Structure–electronic synthesis design of deployable truss antenna. *Aerosp Sci Technol* 26:259–267
5. Gosselin CM, Gagnon-Lachance D (2006) Expandable polyhedral mechanisms based on polygonal one-degree-of-freedom faces. *Proc Inst Mech Eng Part C J Mech Eng Sci* 220:1011–1018
6. Kiper G, Söylemez E, Kişisel A (2008) A family of deployable polygons and polyhedral. *Mech Mach Theory* 43:627–640
7. Wei GW, Ding XL, Dai JS (2011) Geometric constraint of an evolved deployable ball mechanism. *J Adv Mech Des Syst Manuf* 5:302–314
8. Ding XL, Yang Y, Dai JS (2013) Design and kinematic analysis of a novel prism deployable mechanism. *Mech Mach Theory* 63:35–49
9. Zheng F, Chen M (2015) New conceptual structure design for affordable space large deployable antenna. *IEEE Trans Antennas Propag* 63:1351–1358
10. You Z (2000) Deployable structure of curved profile for space antennas. *J Aerosp Eng* 13:139–143
11. Dai L, Guan FL, Guest James K (2014) Structural optimization and model fabrication of a double-ring deployable antenna truss. *Acta Astronaut* 94:843–851
12. Tanaka H (2006) Design optimization studies for large-scale contoured beam deployable satellite antennas. *Acta Astronaut* 58:443–451
13. Yu Y, Luo YZ (2009) Motion analysis of deployable structures based on the rod hinge element by the finite particle method. *Proc Inst Mech Eng Part C J Aerosp Eng* 223:955–964
14. Zhao ML, Guan FL (2005) Kinematic analysis of deployable toroidal spatial truss structures for large mesh antenna. *J Int Assoc Shell Spatial Struct* 46:195–204
15. Xu Y, Guan FL, Zheng Y, Zhao ML (2012) Kinematic analysis of the deployable truss structures for space applications. *J Aerosp Technol Manage* 4:453–462
16. Xu Y, Guan FL, Chen JJ, Zheng Y (2012) Structural design and static analysis of a double-ring deployable truss for mesh antennas. *Acta Astronaut* 81:545–554
17. Li TJ, Wang Y (2009) Deployment dynamic analysis of deployable antennas considering thermal effect. *Aerosp Sci Technol* 13:210–215
18. Li TJ (2012) Deployment analysis and control of deployable space antenna. *Aerosp Sci Technol* 18:42–47